Supplementary Information
List

Supplementary Figure 1. Tumor histology of human and mouse HCCs and characterization of CD133+/CD49f+ liver tumor-initiating cells (TICs) isolated from mouse and human HCCs.

Supplementary Figure 2. TLR4-dependent tumor growth and histology of xenograft tumors derived from TICs from ethanol-fed HCV *Core* Tg mice.

Supplementary Figure 3. Roles of NANOG vs. NANOGP8 in tumorginetic activity of TICs.

Supplementary Figure 4. Low TIC percentage in xenograft-derived tumros and minimal contributions of CD24 to TIC's tumorigenic activity.

Supplementary Figure 5. Expression of YAP1 and IGF2BP3 inhibits TGF-β-signaling and is associated with stemness gene expression.

Supplementary Figure 6. Increased TLR4 immunostaining of subcutaneous tumors generated with Huh7 cells transduced with *SPNB* shRNA.

Supplementary Figure 7. YAP1 and IGF2BP3 immunoreactivity in human HCC and non-HCC liver tissues.

Supplementary Figure 8. *Yap1* and *Igf2bp3* silencing promotes growth inhibition and cell death induced by chemotherapeutic drugs.

Supplementary Table 1. Microarray results, listing differentially regulated genes in TICs.

Supplementary Table 2. CD133+/CD49f+ cells derived from alcohol-fed HCV *Ns5a* Tg mice display tumor-initiating properties

Supplementary Table 3. Clinicopathological features of patients with hepatocellular carcinoma (HCC).

Supplementary Table 4. Clinicopathological features of human HCC and non-HCC patients.

Supplementary Materials and Methods
Supplementary References

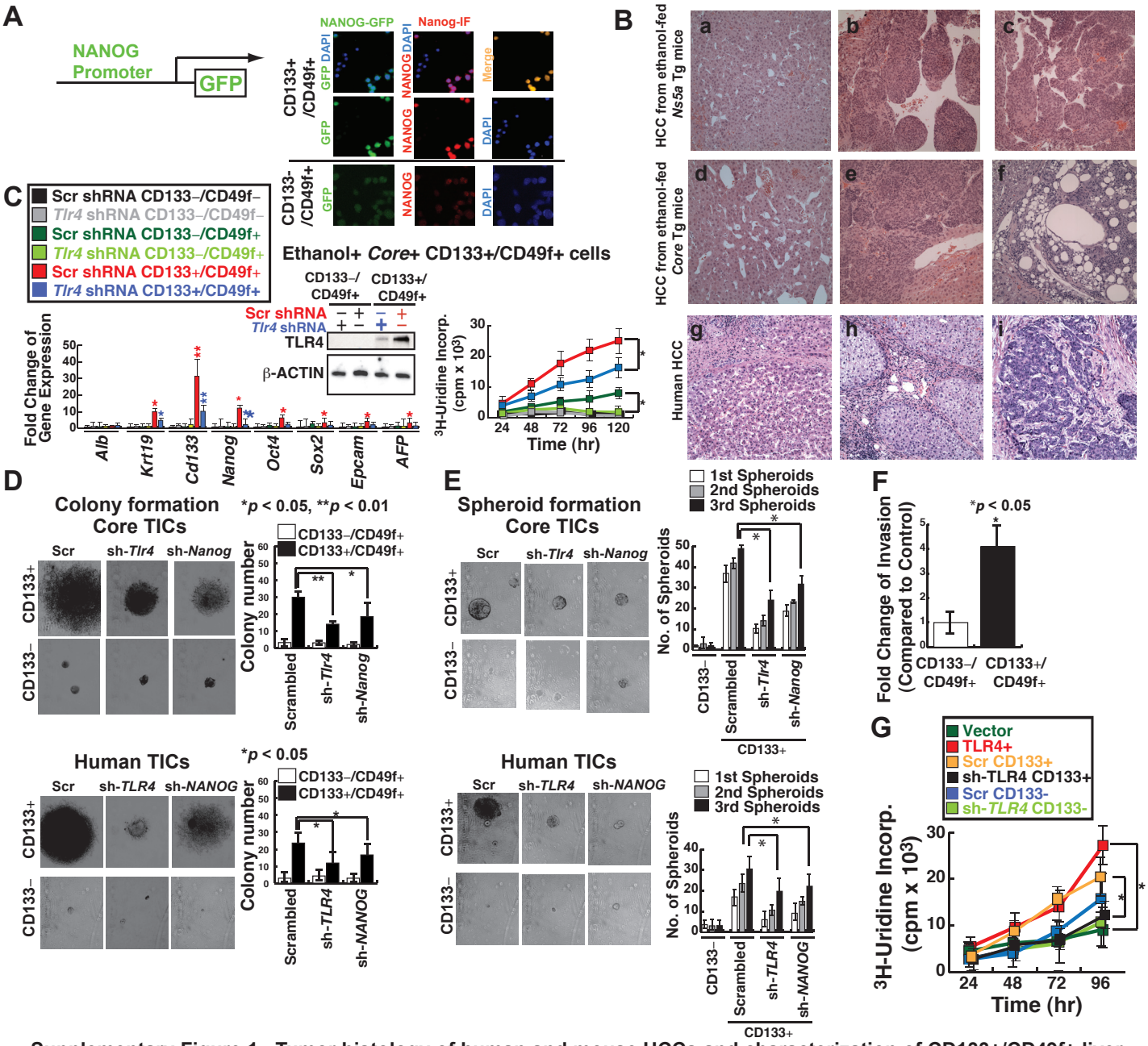

Supplementary Figure 1. Tumor histology of human and mouse HCCs and characterization of CD133+/CD49f+ liver tumor-initiating cells (TICs) isolated from mouse and human HCCs. (**A**) Fluorescence images of *NANOG*-promoter-driven GFP expression and PE-conjugated antibody-based immunostaining of NANOG in CD133-/CD49f+ vs. CD133+/CD49f+ cells from *Ns5a* Tg mice, demonstrating co-localization of both stainings and increased expression of NANOG in CD133+/CD49f+ TICs. (**B**) Hematoxylin-eosin (H&E) staining of liver tumors from alcohol-fed *Ns5a* and *Core* Tg mice and alcoholic HCV patients (**a-i**). These tumors show 3 different growth patterns, namely, (**a,d,g**) thin cords of liver cells, resembling normal liver parenchyma; (**b,e,h**) a broad sheet of cells with a nodular pattern; and (**c,f,i**) a ductal pattern. Magnification: 200 X. (**C**) TICs isolated from alcohol-fed HCV *Core* Tg mice express higher levels of *Nanog*, *Oct4*, *Sox2*, and cytokeratin-19 (*Krt19*), than CD133−/CD49f+ or CD133-/CD49f- cells as determined by qPCR. Immunoblots reveal increased TLR4 protein levels in TICs, which are effectively silenced by transduction of TLR4 directed lentiviral shRNA (**insets**). TLR4 silencing abrogates induction of stemness gene expression. (**D**) Both mouse (**Top**) and human (**Bottom**) TICs but not CD133- control cells form colonies in soft agar, and the numbers of colonies formed are significantly reduced by transduction of shRNA against TLR4 or NANOG. (**E**) Spheroids are formed by TICs but not by control cells. The spheroid formation is reduced in sh-*Tlr4* or sh-*Nanog*-transduced mouse (**Top**) and human (**Bottom**) TICs. Secondary and tertiary spheroid formation from the cells dissociated from spheroids, also demonstrate less serial spheroid-forming capacity in sh-*TLR4* or sh-*NANOG*-transduced TICs. (**F**) Invasiveness of TICs is 4-fold higher than that of control cells (*$p < 0.05$), as evaluated by a Matrigel assay using 8.0-μm pore FluoroBlok inserts. (**G**) ^{3}H-uridine incorporation assays demonstrate enhanced proliferation of TLR4-transduced Huh7 cells and reduced proliferation of CD133+ Huh7 cells upon TLR4 silencing (*$p<0.05$).

Supplementary Figure 1
Chen *et al*.

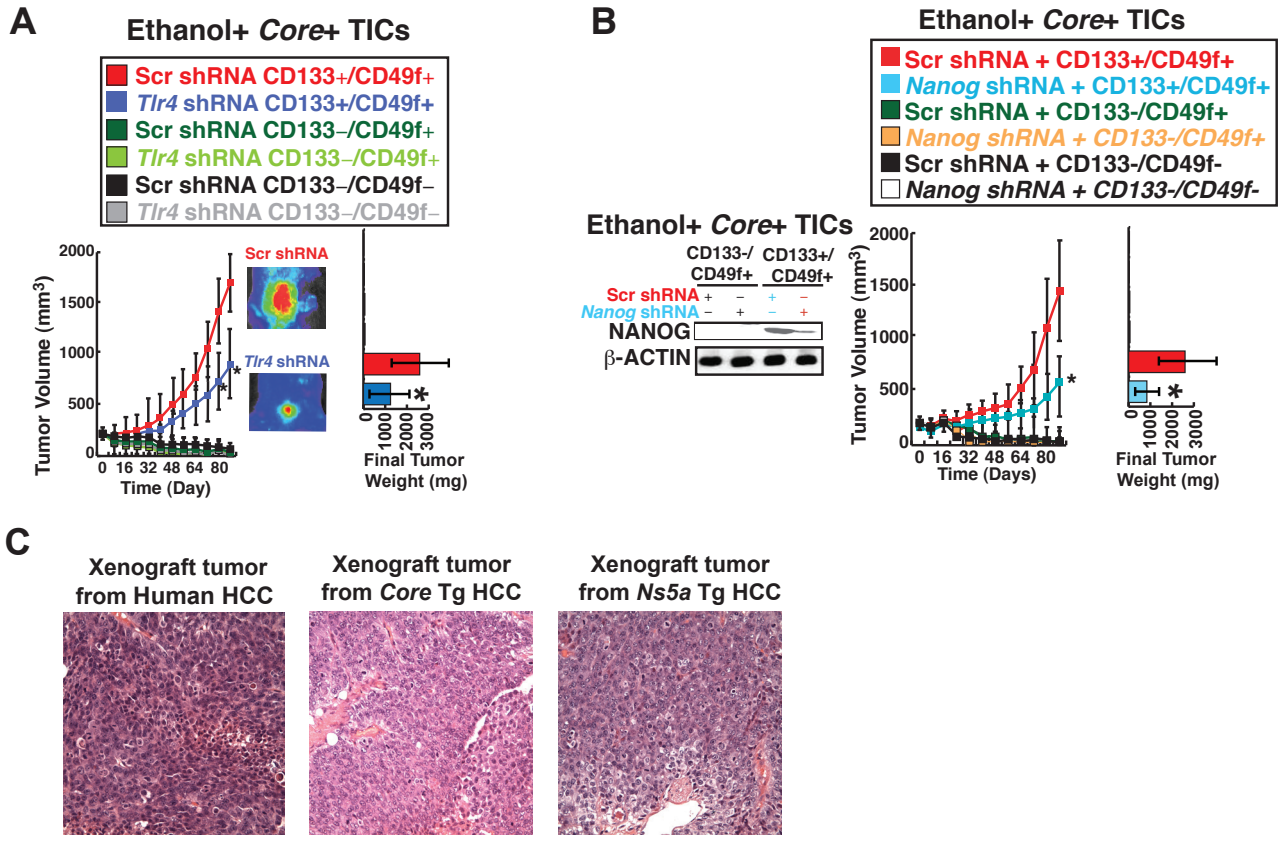

Supplementary Figure 2. TLR4-dependent tumor growth and histology of xenograft tumors derived from TICs from ethanol-fed HCV *Core* Tg mice. (**A**) GFP-transduced TICs, but not other populations from the HCV *Core* Tg mice, give rise to growing tumors following subcutaneous transplantation into NOG mice, as determined by whole body imaging. Tumor growth is attenuated by *Tlr4* shRNA transduction prior to transplantation (*p<0.05). Similarly, final tumor weight is reduced with *Tlr4* shRNA (bar graphs). (**B**) Tumor growth and final tumor weight (bar graphs) are attenuated in all three groups by Nanog shRNA transduction prior to transplantation (*p<0.05). (**Inset**) NANOG protein expression is reduced by lentiviral shRNA knockdown in TICs. (**C**) H&E stained sections of subcutaneous tumors derived from xenograft transplantation of TICs isolated from human HCC, Core or *Ns5a* Tg mice.

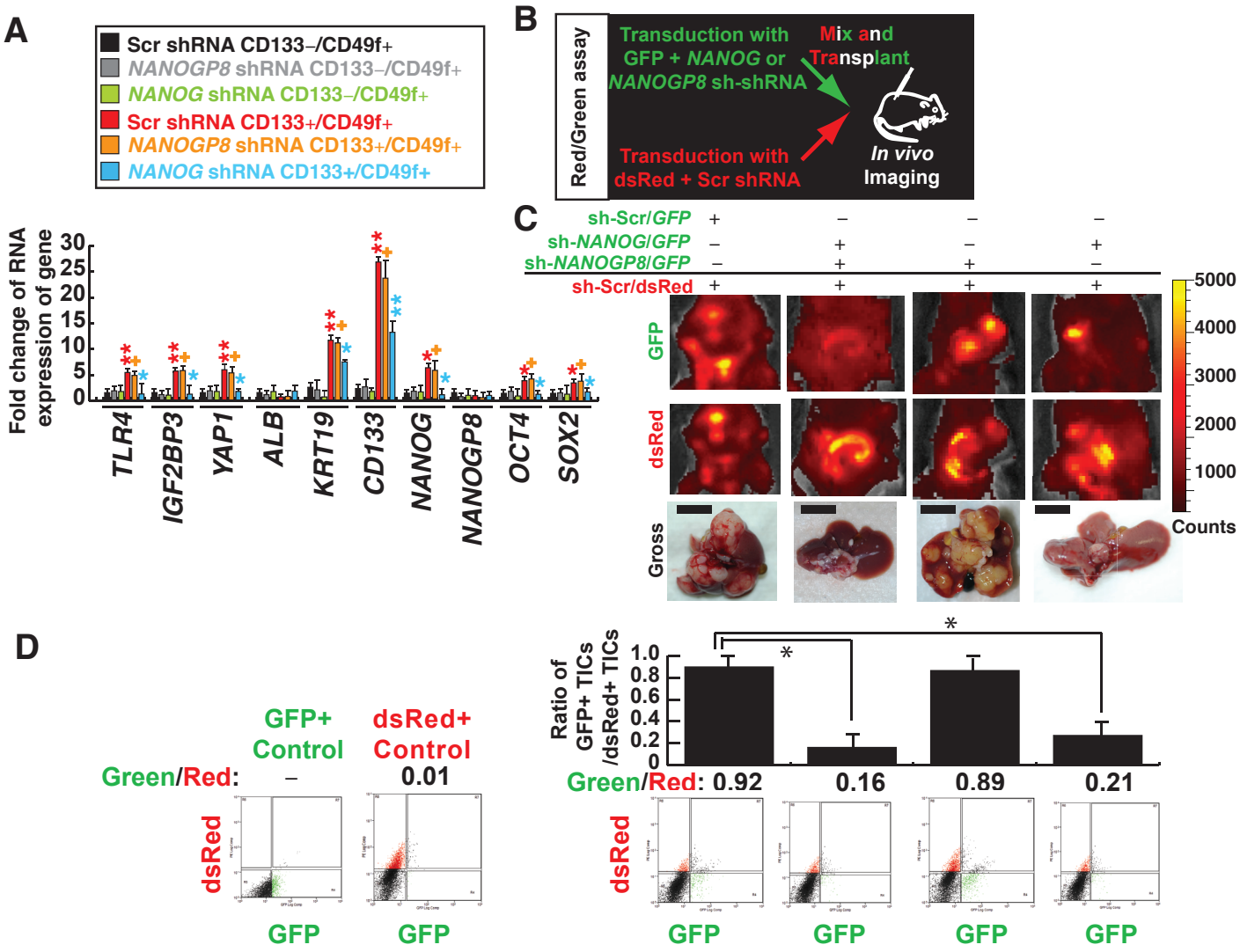

Supplementary Figure 3. Roles of NANOG vs. NANOGP8 in tumorginetic activity of TICs. (**A**) Silencing of NANOG but not NANOGP8 reduces the expression of stemness genes (*CD133*, *NANOG*, *OCT4* and *SOX2*) and oncogenes (*IGF2BP3* and *YAP1*) in TICs isolated from HCC from an alcoholic HCV patient. **p*<0.05 and ***p*<0.01 compared to the control cells; +*p*<0.05 compared to scrambled (Scr) shRNA-transduced TICs. (**B**) A scheme of the TIC orthotopic transplnatation competition assay: Human TICs are infected with lentivirus expressing *NANOG* shRNA, *NANOGP8* shRNA, or scrambled shRNA with GFP. These cells and TICs transduced with scrambled shRNA and dsRed were mixed at the ratio of 1:1, and 10^5 cels were injected into the spleen of C57Bl/6 mice to assess tumor growth by dsRed/GFP dual whole-body imaging. (**C**) Representative images depicting GFP and dsRed-labeled tumor growth of TICs, which is only attenuated when the injected cells include *NANOG* shRNA/GFP+ cells but not *NANOGP8* shRNA/GFP+ cells. In line with these data, gross photos from the respective excised livers also indicate that *NANOG* shRNA/GFP+ cells result in minimal tumor growth. (**D**) FACS plots of *in vivo* red/green assays in xenografts of TICs with GFP+ populations expressing scrambled shRNA, sh-*NANOGP8*, and sh-*NANOG* vs. a dsRed+ TICs population expressing scrambled shRNA. Quantification of FACS ratios in red/green competition assays in vivo after normalization with controls, which are set to 1. After xenotransplantation, GFP+ cells with *NANOG* knockdown disappear. Tumours are composed exclusively of Scr shRNA-transduced dsRed+ control cells. Asterisks denote significant changes: **p*<0.05.

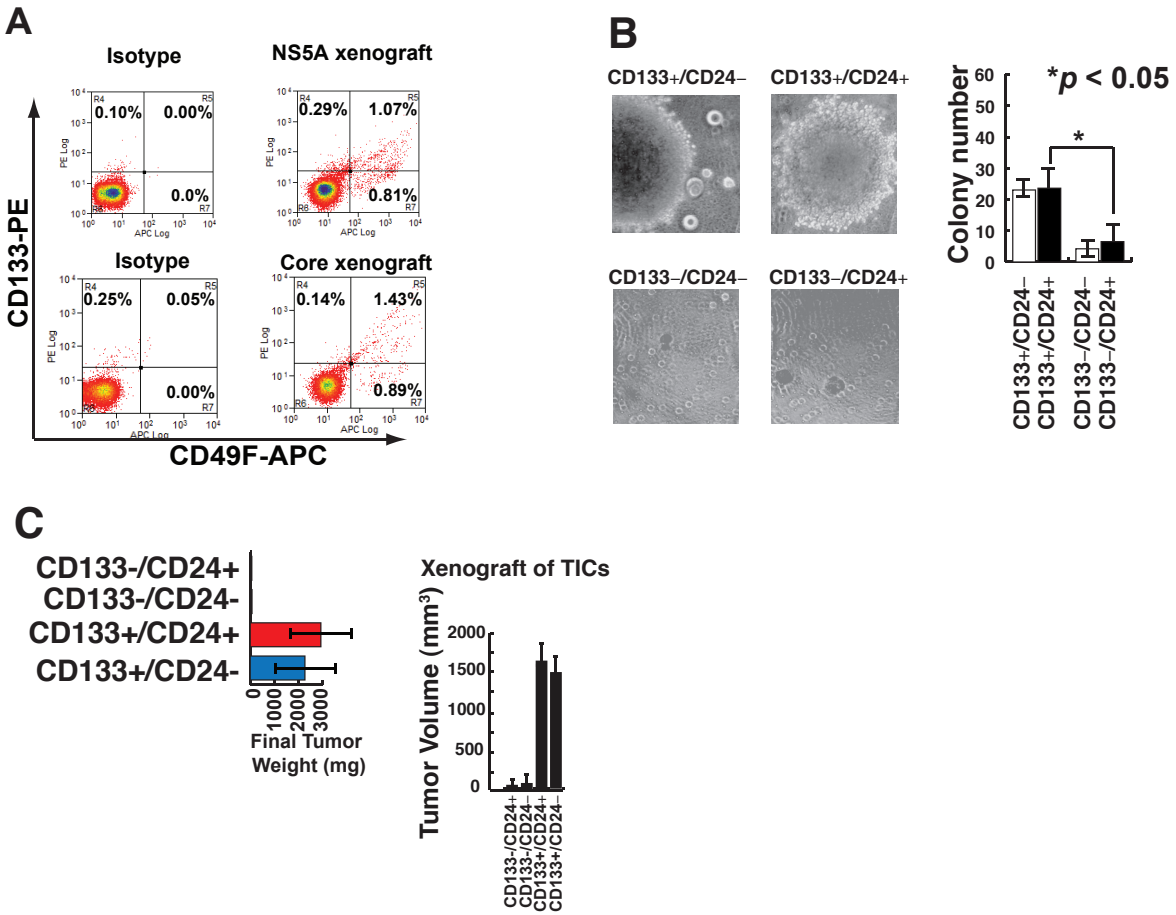

D

Tumor-driver gene candidates in NANOG-negative control CD133-/CD49f+ cells from HCV *Ns5a* Tg mice fed alcohol for 12 months

Gene name	Full name	Function	Gene accession number
Trim16	Tripartite motif protein 16	Stabilization of estrogen receptor, zinc finger protein	NM_053169
Tnfaip6	TNF α-induced protein 6 (TSG6)	Extracellular matrix stability and cell migration	NM_009398

Candidate genes were identified by lentivirus cDNA screening in mouse oval cell lines

Supplementary Figure 4. Low TIC percentage in xenograft-derived tumros and minimal contributions of CD24 to TIC's tumorigenic activity.

(**A**) The percentage of CD133+/CD49f+ cells are analyzed by dissociating the cells from tumors developed from TICs in immunocompromised NOG mice and subjecting them to FACS analysis. (**B**) Colony formation assays demonstrate that CD133+/CD24+ and CD133+/CD24- TICs are not different regarding colony forming ability. (**C**) Xenograft transplantation of CD133+/CD24+ or CD133+/CD24- cells produces subcutaneous tumors with similar weight and size. (**D**) Only two genes were isolated and sequenced from colonies transduced by the control cell (CD133-/CD49f+) cDNA library.

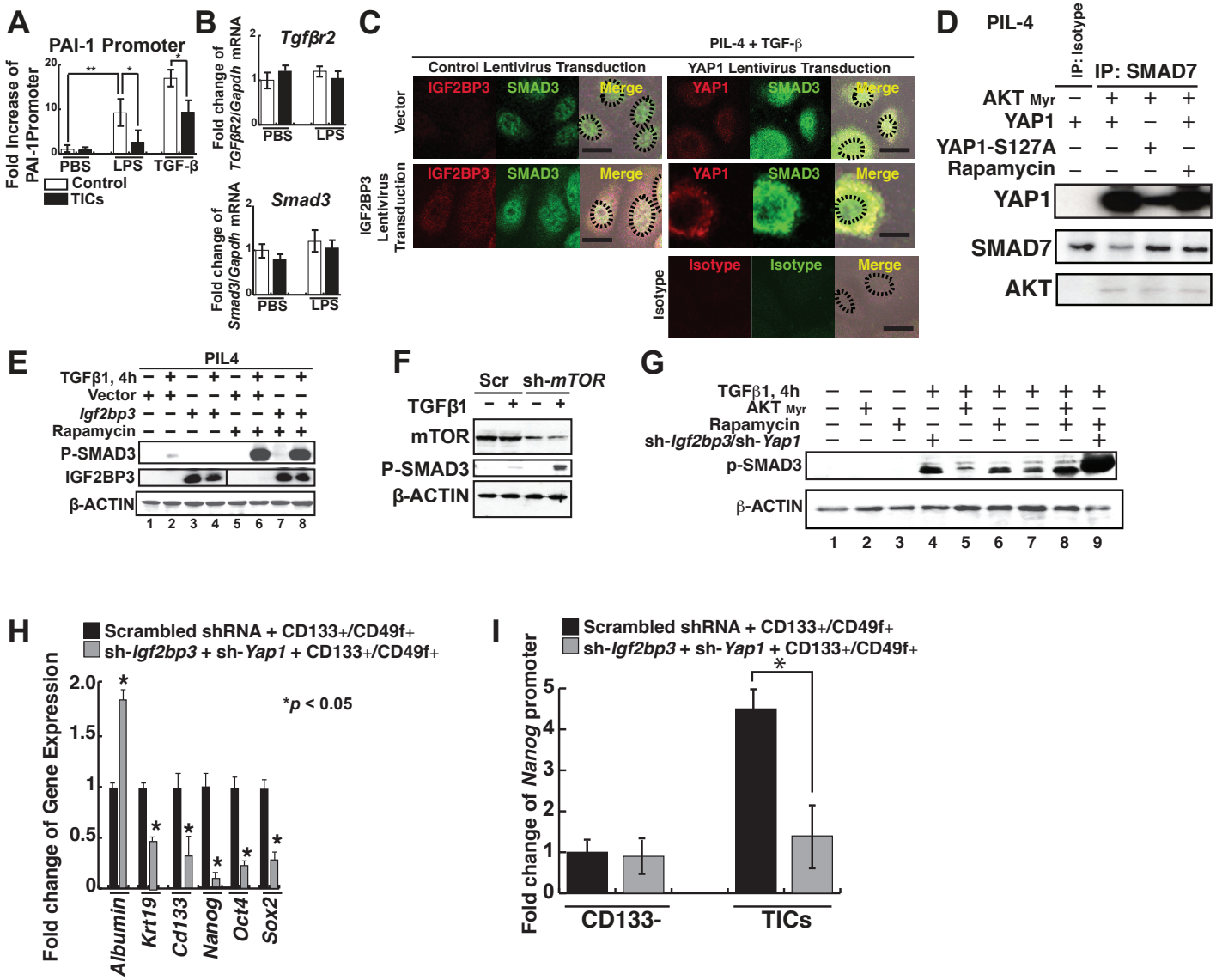

Supplementary Figure 5. Expression of YAP1 and IGF2BP3 inhibits TGF-β-signaling and is associated with stemness gene expression. (**A**) LPS- or TGF-β-induced PAI-1 promoter activity is attenuated in TICs from the Ns5a Tg model as compared to CD133- control cells. *p<0.05 (**B**) mRNA levels for *Tgfβr2* and *Smad3* are not different between TICs and control cells. (**C**) Immunofluorescence microscopy of SMAD3 in TGF-β-treated PIL-4 cells overexpressing YAP1 and/or IGF2BP3. Note, TGF-β-induced nuclear localization of SMAD3 in mock-infected cells is no longer observed upon *Yap1* or/and *Igf2bp*3 transduction. Scale bar = 10μm. (**D**) Co-immunoprecipitation analysis demonstrates that YAP1 strongly interacts with SMAD7 in PIL-4 cells transduced with *Yap1* or constitutively active myristoylated AKT (AKT Myr). This interaction is reduced by overexpression of an S127A mutant of YAP1, but not by rapamycin. (**E**) TGF-β-induced SMAD3 phosphorylation is inhibited by IGF2BP3 but augmented by rapamycin treatment in PIL4 cells. (**F**) Silencing of mTOR with shRNA increases TGF-β induced p-SMAD3 levels in TICs. (**G**) Rapamycin and shRNA-based knockdown of *Igf2bp3*/*Yap1* have a synergistic positive effect on TGF-β-induced p-SMAD3 levels in TICs. (**H**) Expression of stemness genes but not albumin is inhibited by transduction of shRNA against *Igf2bp3* and *Yap1* in TICs, as determined by qRT-PCR. (**I**) *Nanog* promoter analysis with a *Nanog*-promoter luciferase reporter construct demonstrates that silencing of *Yap1*/*Igf2bp3* reduces the promoter activity, indicating that a positive amplification loop exists between NANOG and YAP1/IGF2BP3 pathways.
* p<0.05.

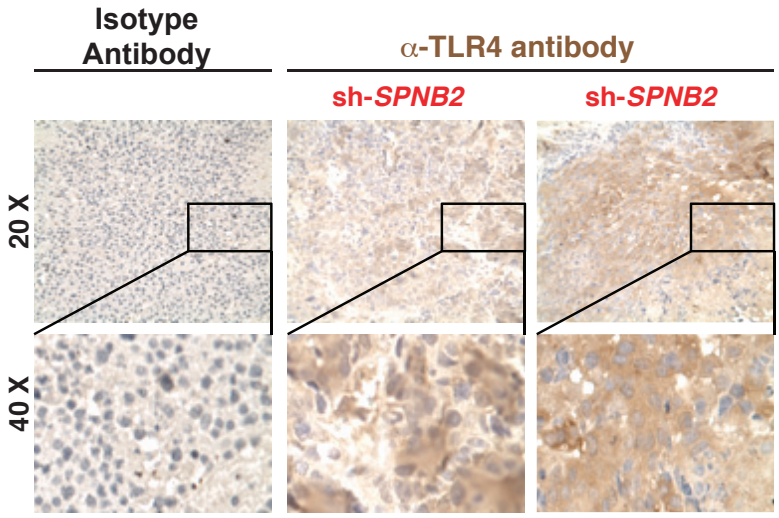

Supplementary Figure 6. Increased TLR4 immunostaining of subcutaneous tumors generated with Huh7 cells transduced with *SPNB2* shRNA.

Suppl. Fig. 6.
Chen *et al*.

A

Semiquantitation of IGF2BP3 or YAP1 Immunoreactivity in Non-tumorous Liver and HCC from Patients with HCV Infection and/or Alcoholism

Condition	Specimens anlyzed (*n*)	Specimens with IGF2BP3 Immunoreactivity score (n)					Frequency of 2 or more
		0	1 (+)	2 (++)	3 (+++)	4 (++++)	
Non-tumorous liver	29	16	8	4	0	0	3/28
HCC	34	4	5	10	9	6	26/34

Condition	Specimens anlyzed (*n*)	Specimens with Yap1 Immunoreactivity score (n)					Frequency of 2 or more
		0	1 (+)	2 (++)	3 (+++)	4 (++++)	
Non-tumorous liver	29	20	6	2	0	0	6/29
HCC	34	4	3	9	10	8	25/34

B

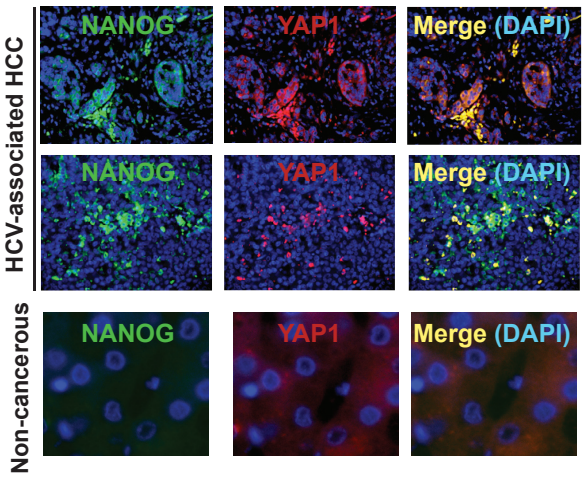

C

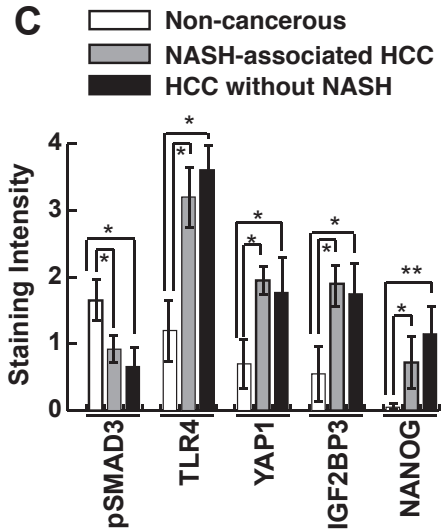

Supplementary Figure 7. YAP1 and IGF2BP3 immunoreactivity in human HCC and non-HCC liver tissues. (**A**) Semiquantitation of IGF2BP3 or YAP1 immunoreactivity in non-tumorous liver and HCC tissues from patients with HCV infection and/or alcoholism. (**B**) Immunofluorescence staining for NANOG and YAP1 is increased in HCC as compared to non-cancerous tissues. (**C**) Staining intensities of TLR4, YAP1, IGF2BP3, and NANOG are all increased in HCC with or without NASH compared to non-cancerous liver tissues. Conversely, p-SMAD3 staining is reduced in HCC. * $p < 0.05$.

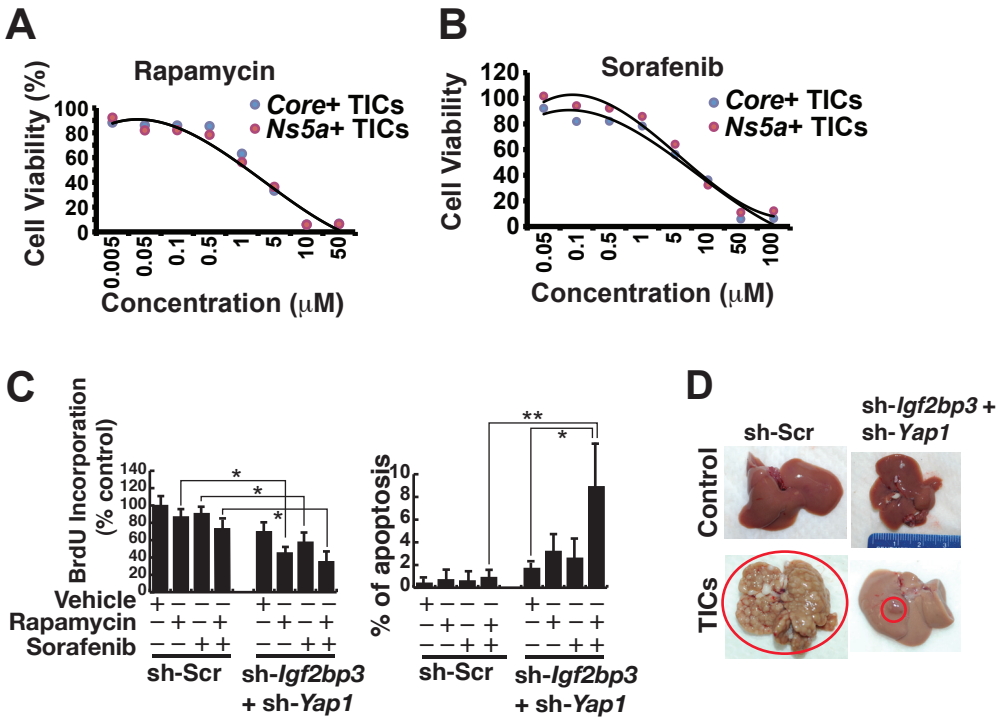

Supplementary Figure 8. *Yap1* and *Igf2bp3* silencing promotes growth inhibition and cell death induced by chemotherapeutic drugs. (**A, B**) Rapamycin or Sorafenib reduces the viability of TICs isolated from HCV *Core* or *Ns5a* Tg mice in a concentration-dependent manner in culture. (**C**) *Igf2bp*3 or/and *Yap1* silencing potentiates the inhibitory efffect of rapamycin or sorafenib on TIC cell proliferation in culture as assessed by BrdU incorporation (**left**). This effect is associated with increased apoptotic cell death of TIC, as assessed by TUNEL assay (**right**). (**D**) Representative photos depict that *Igf2bp3*/*Yap1* silencing markedly reduces the size of tumors generated from TICs injected into the spleen of C57Bl/6 mice treated with the chemotherapeutic drugs as opposed to scramble shRNA transduction.

Supplementary Figure 8
Chen *et al*.

Supplementary Table 1. Microarray results listing differentially regulated genes in TICs

Gene Symbol	Gene Description	Accession Number	Fold Change
D4300 19H16Rik	RIKEN cDNA D4300 19H16 gene	NR_0154 81	14.17
Ogn	osteoglycin	NM_008760	11.98
Ogn	osteoglycin	NM_008760	11.16
8430406P12Rik	RIKEN cDNA 8430406P12 gene	---	10.20
Rgs4	regulator of G-protein signaling 4	NM_009062	9.72
Tnfrsf21	tumor necrosis factor receptor superfamily, member 21	NM_178 589	8.37
Zfp568	zinc finger protein 568	NM_001033 355	8.16
Arhgap20	Rho GTPase activating protein 20	NM_175535	7.75
Phox2b	paired-like homeobox 2b	NM_008888	7.65
Sema3d	sema domain, immunoglobulin domain (Ig), short basic domain	NM_028 882	6.92
Slc6a4	solute carrier family 6 (neurotransmi tter transporter, serotonin)	NM_010 484	6.83
Fgg	fibrinogen gamma chain	NM_133862	6.72
Fmo2	flavin containing monooxygenase 2	NM_018881	6.70
Fmo2	flavin containing monooxygenase 2	NM_018881	6.64
Rnasel	ribonuclease L (2', 5'-oligoisoadenylate synthetase-dependent)	NM_011 882	6.59
Fzd3	frizzled homolog 3 (Drosophila)	NM_021458	6.21
Il33	interleukin 33	NM_0011647 24	6.19
Sprr2a1 /// Sprr2a2	small proline-rich protein 2A1 /// small proline-rich protein 2A2	NM_001164 787	6.15
Bace2	beta-site APP-cleaving enzyme 2	NM_019517	6.10
Bace2	beta-site APP-cleaving enzyme 2	NM_019517	5.98
Fmo2	flavin containing monooxygenase 2	NM_018881	5.84
Sprr2a1 /// Sprr2a2	small proline-rich protein 2A1 /// small proline-rich protein 2A2	NM_001164 787	5.84
Alg11	asparagine-linked glycosylation 11 homolog	NM_183 142	5.82
Fmo2	flavin containing monooxygenase 2	NM_018881	5.77
Ifi44	interferon-induced protein 44	NM_133871	5.73
Rsl1	regulator of sex limited protein 1	NM_001013769	5.72
Orm1	orosomucoid 1	NM_008768	5.70
Cpm	carboxypeptidase M	NM_027468	5.50
Slc38a1	solute carrier family 38, member 1	NM_001166456	5.47
Esrp1	epithelial splicing regulatory protein 1	NM_194055	5.39
Gprin3	GPRIN family member 3	NM_183183	5.33
Bace2	beta-site APP-cleaving enzyme 2	NM_019517	5.31
Fam108a	family with sequence similarity 108, member A	NM_145421	5.30
Lpl	lipoprotein lipase	NM_008509	4.90
Dlg2	discs, large homolog 2 (Drosophila)	NM_011807	4.87
Rsad2	radical S-adenosyl methionine domain containing 2	NM_021384	4.83
Mpp3	membrane protein, palmitoylated 3 (MAGUK p55 subfamily member 3)	NM_007863	4.82
Tfpi2	tissue factor pathway inhibitor 2	NM_009364	4.67
Kctd12b	potassium channel tetramerisation domain containing 12b	NM_175429	4.66
Gata4	GATA binding protein 4	NM_008092	4.58
Dio2	deiodinase, iodothyronine, type II	NM_010050	4.58
Il10	interleukin 10	NM_010548	4.56
LOC100048346 /// Usp18	similar to ubiquitin specific protease UBP43 /// ubiquitin specific peptidase 18	NM_011909	4.55
Tmem51	transmembrane protein 51	NM_145402	4.52
Rsad2	radical S-adenosyl methionine domain containing 2	NM_021384	4.47
Bace2	beta-site APP-cleaving enzyme 2	NM_019517	4.43
Rasl11a	RAS-like, family 11, member A	NM_026864	4.40
Hhip	Hedgehog-interacting protein	NM_020259	4.38
Tiam1	T-cell lymphoma invasion and metastasis 1	NM_001145886	4.32
Atp1b2	ATPase, Na+/K+ transporting, beta 2 polypeptide	NM_013415	4.27
Aox3	aldehyde oxidase 3	NM_023617	4.17
Fga	fibrinogen alpha chain	NM_001111048	4.17
Trim63	tripartite motif-containing 63	NM_001039048	4.16
Spry3	sprouty homolog 3 (Drosophila)	NM_001030293	4.12
1110020G09Rik	RIKEN cDNA 1110020G09 gene	NM_001040395	4.11
Kctd12b	potassium channel tetramerisation domain containing 12b	NM_175429	4.07
Parm1	prostate androgen-regulated mucin-like protein 1	NM_145562	4.05

Supplementary Table 1. Microarray results listing differentially regulated genes in TICs (Continued)

Gene Symbol	Gene Description	Accession Number	Fold Change
Gas5	growth arrest specific 5	NR_002840	0.25
Spink10	serine peptidase inhibitor, Kazal type 10	NM_177829	0.25
Prdm1	PR domain containing 1, with ZNF domain	NM_007548	0.24
Fbp2	fructose bisphosphatase 2	NM_007994	0.24
Zfr	zinc finger RNA binding protein	NM_011767	0.24
Ncam1	neural cell adhesion molecule 1	NM_001081445	0.24
Akr1b10	aldo-keto reductase family 1, member B10 (aldose reductase)	NM_172398	0.24
Tcf12	Transcription factor 12	NM_011544	0.23
Amz1	archaelysin family metallopeptidase 1	NM_173405	0.23
B230117O15Rik	RIKEN cDNA B230117O15 gene	---	0.22
Neo1	neogenin	NM_001042752	0.21
7030407O06Rik	RIKEN cDNA 7030407O06 gene	---	0.21
Xpo7	exportin 7	NM_023045	0.21
Usp40	ubiquitin specific peptidase 40	NM_001033291	0.20
Dtl	denticleless homolog (Drosophila)	NM_029766	0.20
Acaa1b	acetyl-Coenzyme A acyltransferase 1B	NM_146230	0.20
Angptl4	angiopoietin-like 4	NM_020581	0.19
Klhl30	kelch-like 30 (Drosophila)	NM_027551	0.19
Rbm3	RNA binding motif protein 3	NM_001166409	0.18
BC080696	cDNA sequence BC080696	XR_001743	0.18
Angptl6	angiopoietin-like 6	NM_145154	0.15
Npr3	natriuretic peptide receptor 3	NM_001039181	0.15
AU018091	expressed sequence AU018091	NM_001004153	0.14
Chn1	chimerin (chimaerin) 1	NM_001113246	0.14
Smc6	structural maintenance of chromosomes 6	NM_025695	0.13

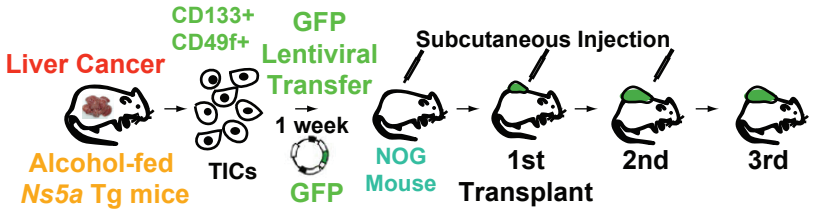

Supplementary Table 2. CD133+/CD49f+ cells derived from alcohol-fed HCV *Ns5a* Tg mice display tumor-initiating properties

Genotype	Diet (12 months)	shRNA	No. of cells injected	Fraction of injected NOD/Scid/Il2γ −/− mice bearing tumors after 3 months					
				1st transplant			2nd transplant	3rd transplant	
				Tumor bulk	CD133+ CD49f+	CD133- CD49f+	CD133+ CD49f+	CD133+ CD49f+	Ratio of TICs
Ns5a Tg-1	Alcohol	−	10,000	0/6	6/6	0/6	4/6	3/6	
			2,500	0/6	3/6	0/6	2/6	2/6	1/1615 - 1/7337
			500	0/6	0/6	0/6	n.d.	n.d.	
Ns5a Tg-2	Alcohol	−	10,000	0/6	5/6	0/6	3/6	2/6	
			2,500	0/6	2/6	0/6	2/6	1/6	1/2875 - 1/13723
			500	0/6	0/6	0/6	n.d.	n.d.	
Ns5a Tg-3	Alcohol	−	10,000	0/6	6/6	0/6	3/6	3/6	
			2,500	0/6	4/6	0/6	3/6	2/6	1/1243 - 1/5811
			500	0/6	0/6	0/6	n.d.	n.d.	
Ns5a Tg	Alcohol	Scrambled	10,000	0/6	6/6	0/6	4/6	3/6	
			2,500	0/6	4/6	0/6	3/6	2/6	1/1243 - 1/5811
			500	0/6	0/6	0/6	n.d.	n.d.	
Ns5a Tg	Alcohol	+ sh-TLR4	10,000	0/6	3/6	0/6	1/6	1/6	
			2,500	0/6	2/6	0/6	1/6	1/6	1/4701 - 1/28914
			500	0/6	0/6	0/6	n.d.	n.d.	
Ns5a Tg	Alcohol	+ sh-NANOG	10,000	0/6	4/6	0/6	2/6	1/6	
			2,500	0/6	2/6	0/6	2/6	1/6	1/3737 - 1/19784
			500	0/6	0/6	0/6	n.d.	n.d.	

Supplementary Table 3. Clinicopathological Features of Patients with Hepatocellular Carcinoma (HCC)

Feature	Value
Age (years) (Mean ± S.D.)	55.3 ± 11.6
Gender	
Male	21
Female	13
Noncancerous liver tissue	
Normal liver	19
Inflammatory liver	10
Number of tumor	
Solitary	15
Multiple	19
Tumor differentiation	
Well	5
Moderately	7
Poorly	4
Unknown	5

Supplementary Table 3
Chen *et al*.

Supplementary Table 4. Clinicopathological Features of Human HCC and Non-HCC Patients

Patient Code	HCV	Alcoholism	Diagnosis	Histopathology	Gender/ Age (yr)	Degree of Differentiation	Cell Pattern	Capsular Invasion	Portal-vein Invasion
HCC-2342	+	+	HCC I (2 / 0.8 cm)	Angiolymphotic invasion	M/45	Moderate	Trabecular	+	+
HCC-5425	+	+	HCC III (2.5 / 2 / 1.8 cm)	Cirrhosis, Partial necrosis	M/68	Poor	Trabecular	–	-
HCC-3258	+	–	HCC 0 (3.2 / 1.5 cm)	Cirrhosis	F/67	Moderate	Trabecular	+	–
HCC-8904	+	+	HCC (1 / 1.3 cm)	Cirrhosis,	M/57	Well	Pseudoglandular	+	–
HCC-2638	–	+	HCC (3 / 1.6 cm)	Primary biliary cirrhosis	M/53	Well	Trabecular	–	–
HCC-5568	+	–	HCC I (2.8 cm)	Partial necrosis	M/45	Moderate	Trabecular	-	–
HCC-1287	+	-	HCC (6/4/2/2/2 cm)	Cirrhosis, Partial necrosis	M/68	Poor	Trabecular	–	-
HCC- 6945	+	–	HCC 0 (7.6 / 1.3 cm)	Cirrhosis	M/56	Poor	Trabecular	–	–
HCC- 5481	+	–	HCC (5 cm)	Tumor necrosis	M/57	Moderate	Pseudoglandular	–	–
HCC-2387	+	–	HCC (0.3 cm)	Cirrhosis Inflamamtion	M/53	Well	Pseudoglandular	–	–
HCC-5874	–	–	HCC (2 / 0.8 cm)	Angiolymphotic invasion	M/67	Poor	Trabecular	–	–
HCC-9693	–	-	HCC (4.5 cm)	Tumor necrosis	M/78	Moderate	Trabecular	–	–
HCC-5428	–	+	HCC (3 / 1 cm)	Partial necrosis	M/52	Moderate	Trabecular	–	+
HCC-3628	–	+	HCC (2 / 1.5 / 1.5 cm)	Angiolymphotic invasion	F/65	Poor	Trabecular	–	+
HCC-6287	–	-	HCC (2.5 cm)	Angiolymphotic invasion	F/63	Well	Trabecular	–	+
HCC-3602	–	-	HCC (3.8 / 3.2 / 3.2 cm)	Cirrhosis	M/61	Poor	Trabecular	–	+
HCC-0278	–	+	HCC (0.7 cm)	Partial necrosis	F52	Well	Trabecular	–	-
HCC-0398	–	+	HCC (1.6 cm)	Cirrhosis	F/60	Well	Trabecular	–	-
HCC-3698	–	-	HCC (1.2 cm)	Partial necrosis	F/49	Well	Trabecular	–	-
HCC-2013	+	+	HCC (1.4 cm)	Cirrhosis	M/80	Well	Pseudoglandular	–	-
HCC-2036	–	+	HCC (2 / 0.8 cm)	Angiolymphotic invasion	M/67	Moderate	Trabecular	–	–
HCC-3782	–	-	HCC (3 cm)	Cholangititis, Diabetes	F/42	Moderate	Trabecular	–	–
HCC-0192	+	+	HCC (2.7/2.5/1.8 cm)	Partial necrosis	M/50	Poor	Trabecular	–	+
HCC-3746	+	-	HCC (5/3.5/3.5 cm)	Cholelithisis	M/68	Poor	Pseudoglandular	–	+
HCC-7463	–	–	HCC (3/4 cm)	Cryptogenic cirrhosis	M/61	Poor	Trabecular	–	–
HCC-3722	+	-	HCC (1.1/2 cm)	Cirrhosis	M/61	Moderate	Trabecular	–	–
HCC-0918	+	+	HCC (1.5 / 0.8 cm)	Cryptogenic cirrhosis, NASH	F/58	Moderate	Trabecular	–	+
HCC-7262	–	+	HCC (1.7 / 0.8 cm)	Cryptogenic cirrhosis	F/68	Moderate	Trabecular	–	+
HCC-7209	–	+	HCC (3.2 cm)	Angiolymphotic invasion	F/63	Well	Trabecular	–	+
HCC-3728	–	-	HCC (2.8 / 1.2 cm)	Partial necrosis	M/64	Poor	Pseudoglandular	–	+
HCC-2716	–	+	HCC (1.2 cm)	Partial necrosis	F50	Well	Trabecular	–	-
HCC-8542	+	+	HCC (0.9 cm)	Cirrhosis	F/62	Well	Pseudoglandular	–	-
HCC-5143	–	-	HCC (1.6 cm)	Cirrhosis	M/53	Well	Trabecular	–	-
HCC-3920	–	-	HCC (0.9 cm)	Tumor necrosis	F/80	Well	Pseudoglandular	–	-
Non-HCC-1179	–	-	Cirrhosis	Angiolymphotic invasion	F52	Moderate	Trabecular	–	-
Non-HCC-1323	–	+	Cirrhosis	Cryptogenic	M/67	-	-	–	–
Non-HCC-1287	–	-	Cirrhosis	Cryptogenic	F/63	-	-	–	-
Non-HCC-1203	–	-	-	-	M/58	-	-	–	-
Non-HCC-1141	–	–	Cirrhosis	Cryptogenic	M/57	-	-	–	-
Non-HCC-D767	+	-	Cirrhosis	Cryptogenic	M/58	-	-	–	-
Non-HCC-1653	–	-	Cirrhosis	Cryptogenic	M/60	-	-	–	-
Non-HCC-3928	+	+	Cirrhosis	Angiolymphotic invasion	M/54	-	-	–	-
Non-HCC-1328	–	+	-	Cryptogenic	M/67	-	-	–	–
Non-HCC-1287	+	+	Cirrhosis	-	M/53	-	-	–	-
Non-HCC-9473	–	-	Cirrhosis	Cryptogenic	F/60	-	-	–	-
Non-HCC-6384	–	–	Cirrhosis	Cryptogenic	M/52	-	-	–	-
Non-HCC-1857	+	-	-	Cryptogenic	F/58	-	-	–	-
Non-HCC-1653	–	-	Cirrhosis	-	M/60	-	-	–	-
Non-HCC-3928	–	–	Cirrhosis	-	M/55	-	-	–	-
Non-HCC-1528	–	+	Cirrhosis	Cryptogenic	M/54	-	-	–	–
Non-HCC-1269	–	–	-	Cryptogenic	M/61	-	-	–	-
Non-HCC-2846	–	-	Cirrhosis	-	M/65	-	-	–	-
Non-HCC-1141	+	+	Cirrhosis	Angiolymphotic invasion	M/52	-	-	–	-
Non-HCC-2567	+	-	Cirrhosis	Cryptogenic	F/58	-	-	–	-
Non-HCC-7835	–	-	Cirrhosis	-	M/32	-	-	–	-
Non-HCC-8542	–	–	Cirrhosis	-	M/52	-	-	–	-
Non-HCC-3532	–	+	-	Cryptogenic	F56	-	-	–	–
Non-HCC-1487	–	–	Cirrhosis	Cryptogenic	F/55	-	-	–	-
Non-HCC-1277	+	-	Cirrhosis	Cryptogenic	M/60	-	-	–	-
Non-HCC-2635	+	+	-	-	M/66	-	-	–	-
Non-HCC-3367	–	-	Cirrhosis	-	F/67	-	-	–	-
Non-HCC-1439	–	-	Cirrhosis	Cryptogenic	M/59	-	-	–	-
Non-HCC-7609	–	–	Cirrhosis	-	M/53	-	-	–	-

Supplementary Table 4. Clinicopathological Features of Human HCC and Non-HCC Patients. Clinicopathological information is listed.

Supplementary Materials and Methods

Mice: C57Bl/6 *Ns5a* and *Core* transgenic (Tg) mice (1) and TLR4 mutant mice (C57BL/10ScNJ: Jackson Laboratory) were fed Lieber-DeCarli diets, containing either 3.5% ethanol or isocaloric dextrin (Bioserv, Frenchtown, NJ) for 12 months. Heterozygous knockout of *β2-Spectrin* (*Spnb2*+/-) mice were described previously (2). All animal work was conducted according to national and international guidelines. Animal studies were based on a protocol approved by the Institutional Animal Care and Use Committee at the University of Southern California.

Human subjects: For immunostaining and immunoblotting analysis of IGF2BP3, YAP1 and p-SMAD3 in human HCC, necropsy or surgically excised HCC tissues from 34 patients with or without HCV infection, with or without a history of alcoholism, were obtained as cryo-preserved samples according to the approved University Institutional Review Board (IRB) protocol. Many of the specimens were obtained from Liver Tissue Cell Distribution System at University of Minnesota, University of Southern California, and Harbor UCLA Medical Center. The samples were carefully screened for co-infection with other hepatitis viruses or HIV, as determined by serological tests, as well as for drug addiction and co-morbidities other than alcoholism. Sixteen patients had a history of having more than 4 drinks per day [One drink is described as 12 ounces of beer (5% alcohol), 5 ounces of wine (12% alcohol)] for more than 15 years. Samples were obtained from both genders at the age of 42-80. Histologically, they all had varying degrees of steatosis (microvesicular and macrovesicular) and inflammation in addition to different stages of HCC. Frozen necropsy liver tissues from 29 patients with accidental death or stroke, but without an apparent liver pathology were also obtained for immunostaining or immunoblotting.

Cells: The immortalized mouse liver progenitor *p53*–/– oval cell line PIL-4 was established from *p53*–/– mice by Dr. Aleksandra Filipovska, at the University of Western Australia (3). Mouse NIH3T3 fibroblasts are frequently used for *in vitro* transformation assays to test for proto-oncogenes. This assay is well-established, reproducible, and sensitive to detect subtle oncogenic activity. However, cell-type specificity may become an issue, when exploring the mechanisms of tumorigenesis in liver. About one half of HCC is speculated to arise from an oval cell (progenitor cell) population, and another half from hepatocytes (4, 5). Therefore, PIL-4 cells were used instead of NIH3T3 cells (3). TICs were cultured in DMEM/F12 medium, containing 10% FBS, 1× Nucleosides (Sigma), 100 nM Dexamethasone (Sigma), and 20 ng/ml EGF (Peprotec). PIL-4 cells were cultured in complete Williams E medium (30 ng/ml IGF2, 20 ng/ml EGF, 10 μg/ml Insulin, and 10% fetal bovine serum).

Plasmids, lentivirus and retrovirus vectors, and production of shRNA lentiviruses: The *Ns5a* expression plasmid was constructed by inserting HCV *Ns5a* cDNA downstream of the CMV promoter into pcDNA3.1 (Invitrogen). Expression vectors (pCR2.1-NANOGP8 and pPyCAG-NANOGP8) (6) were generous gifts from Dr. Dean G. Tang (University of Texas, MD Anderson Cancer Center). All retroviruses were based on lentivirus (pPAX2: Addgene) or MMTV vectors (pVPack-GP: Stratagene). Lentivirus vectors were prepared by standard procedures in HEK293T cells. Three plasmids, packaging vector pPAX2, ecotropic envelope gene (VSV glycoprotein) expression vector pMDV (Addgene), and shRNA expression cassette, were transfected in HEK293T cells by lipid-based transfection reagent FuGene6 (Roche). Retrovirus expressing TLR4 was produced in Phoenix cells (7). After 72 hr transfection, the virus supernatant was harvested, mixed with polybrene (4 μg/ml), and used to infect Huh7 cells. The supernatant was harvested, and the virus was purified and titrated.

The following plasmids were obtained from Addgene: pRetroSuper Smad3 (Smad3 shRNA: 15726), pRetroSuper-GFP Smad3 (Smad3 shRNA: 15723), mTOR_2 shRNA (mTOR shRNA:

1856), HA-Akt CA (myr-HA-Akt) (Akt1: 16244), HA-Akt DN (K179M) (Akt1: 16243), pcDNA4/TO/myc-His-A-YAP1 (YAP1: 19059), p2xFLAGhYAP1-S127A (YAP1 isoform, mutant: 17790), MSCV Luciferase PGK-hygro (18782), MSCV IRES Luciferase (18760), pBABE YAP1 (15682), pMXs-Nanog (Nanog homeobox: 13354), and mouse cDNAs encoding *Tlr4* and *Nanog* (Cat #13354, 13578), and MSCV-Luc2p-LC3-IRES-Puro. Myr-Akt consists of Akt1 ligated to a myristoylation sequence, resulting in an enzyme approximately ten-fold more active than the wild-type enzyme (8).

The following plasmids were obtained from Open Biosystems: Human GIPZ lentiviral shRNAmir target gene set for Homo sapiens toll-like receptor 4 (TLR4), transcript variant 4, non-coding RNA (RHS4531-NR_024169, RHS4430-98525129, RHS4430-98843572, RHS4430-99137800). To increase silencing effects and to reduce off-target effects, a combination of shRNA lentiviruses was used to knockdown target genes.

Site-directed mutagenesis was performed according to the PCR-based mutagenesis kit (Quik Change site-directed mutagenesis kit, Stratagene, USA) with Advantage polymerase, (Clontech). Sequences containing a CATT motif are bound by NANOG *in vitro* (9-12). The fragment −978/+55 of the *Igf2bp3* gene, containing putative NANOG binding sites (5'-CATT-3' or 5'-TAAT(G/T)(G/T)-3') was inserted into pGL3 basic vector (*Igf2bp3*-978luc); the same procedure was done for the −1359/+67 fragment of the *Yap1* gene. The *Nanog* consensus sequence CATT was mutated utilizing a mutagenic forward primer and a reverse primer as previously described (13). The mutated sequences were confirmed by DNA sequencing.

The response to TGF-β was measured by infection of adenovirus encoding SBE4-Luc (Smad binding element: 16495, Addgene) or p3TP-Lux (hybrid promoter by fusion of PAI-1 promoter and adenovirus E4 promoter elements driving luciferase reporter gene expression (14).

To address the question of functionality of the two NANOG-encoding genes, *NANOG* and *NANOGP8*, we used specific shRNAs for both. The few bp changes that differentiate the coding sequences of these two genes made it difficult to separately inhibit *NANOGP8 and NANOG*. However, the presence of a small, but unique 3′UTR sequence (6), characteristic for *NANOGP8* finally allowed us to design a lentivector expressing a *NANOGP8*-specific shRNA, and thus, to measure both the combined *NANOG* (*NANOG+NANOGP8*) expression levels as well as the specific levels of *NANOGP8*.

Adenovirus transduction: We also overexpressed a constitutively active (ca) TGF-β type I receptor (caALK-5), using an adenoviral vector (15) to establish the most convenient gain of function, and infected cells were transplanted into mice.

Isolation of mouse and human TICs using FACS: After 12 month-alcohol feeding, *Ns5a* Tg or *Core* Tg mice were sacrificed and liver tumors were digested with collagenase (0.1%) in serum-free DMEM/F-12 media. Resected HCC tissues from patients were immediately dissected into small pieces and similarly digested with collagenase. Suspended liver cells were stained with the following antibodies: PE-anti-CD133, APC-anti-CD49f, and FITC-anti-CD45 (BD Biosciences), followed by FACS analysis. First, CD45+ cells were gated out and CD45− cells were separated by FITC and PE fluorescence intensity. Compensation for FITC, PE, and APC was performed using compensation beads. Analysis was done using the CellQuest program. Positive and negative gates were determined using non-immune IgG-stained and -unstained controls. CD133+/CD49f+ TICs and CD133−/CD49f+ control cells were cryo-preserved in 50% FBS and 10% DMSO.

Human TICs isolation and injection into immunocompromised mice: Tumor and parallel non-tumorous liver tissues were collected from patients who underwent hepatectomy at the time

of operation in the Department of Surgery, USC Hospital, Los Angeles, with Institutional Review Board (IRB) approval and placed into DMEM/F12 medium. The procedure of cell isolation from liver tissues was performed as previously described (16, 17), with some modifications. In brief, after digestion with type IV collagenase (100 units/ml) (Sigma-Aldrich, St. Louis, MO) at 37°C for 15 min, tissues were minced and the cell suspension was passed through a 100 μM nylon mesh (BD Biosciences). After lysis of red blood cells, the remaining cells were counted and subjected to flow cytometry analysis or cell sorting. Male mice, weighing 25–30 g, were purchased from Charles River Labs (Wilmington, MA). Cells were maintained as monolayer culture in DMEM with 10% fetal bovine serum and 1% penicillin (Life Technologies Inc., Carlsbad, CA) at 37°C in a humidified atmosphere of 5% CO_2. Viability of sorted cells was assessed by trypan blue staining, and >80% cell viability was set as requirement for the *in vivo* tumorigenicity assay. Tumorigenicity of CD45−/CD133+/CD49f+ cells isolated from tumor tissues was characterized by injecting the sorted cells into immunodeficient NOG mice. A total of 1×10^4 cells were resuspended in 0.1 ml 1× DMEM/F12 and subcutaneously injected into male NOG mice, aged 6 to 8 weeks. To ensure transduction efficiency of lentiviruses, only infected/shRNA expressing cells were used for transplantation into immunocompromised mice after validation of silencing effects and EGFP positivity sorting by FACS (more than 90% of cells were positive). All the animal experiments were approved by the Committee on IACUC of the University of Southern California. CD133+ and CD133− cells isolated from different tumors were injected subcutaneously into two sides of the same NOG mouse for controlled visualization and comparison. To favor cell growth, the cells isolated from human tumor tissues were injected orthotopically into rear flank regions. In total 1×10^4 tumor cells were injected into immunodeficient mice to serve as a control of cell viability. Animals were sacrificed at the indicated time intervals, when tumor nodules were identified on the body surface of NOG mice (NOD.Cg-*Prkdc*^{scid}-*Il2rg*^{tm1Sug}/JicTac mice: CLEA International, Inc.), or in the liver of C57Bl/6 mice by laparotomy. If tumors were not identified, the abdominal incision was closed by sutures, and the mice were monitored until the second or third time point. In the tumor metastasis model, animals were sacrificed three months after cell injection.

Subcutaneous xenograft transplantation of the TICs into immunodeficient mice: We tested oncogenic activity of *Yap-1* and *Igf2bp3* by xenograft transplantation. CD133+/CD49f+ TICs, CD133−/CD49f+, CD133+/CD49f− or CD133−/CD49f− control cells were infected with lentiviral vectors expressing GFP and shRNA targeting *Yap1*, *Igf2bp3*, both, or scrambled shRNA. Infected cells were mixed with Matrigel (BD Matrigel Matrix High Concentration medium). This method ensures that the injected tumor cells remain localized for *in situ* analysis and/or future excision. At day 10 post lentivirus infection and culture, 6-wk old athymic male nude mice or NOG mice (NOD.Cg-*Prkdc*^{scid}-*Il2rg*^{tm1Sug}/JicTac mice: CLEA International, Inc.) were anesthetized with ketamine (80 mg/kg) and xylazine (10 mg/kg) i.p. The TICs (1×10^4) transduced with lentiviral shRNA (1×10^5 TU/ml: MOI 10) in 0.2 ml medium were injected subcutaneously into the left flank region of athymic male nude mice or NOG mice with Matrigel (Invitrogen). NOG mice that received TICs from *Ns5a* Tg mice were monitored up to 88 days. Ten to twelve mice were tested for each shRNA treatment.

To determine the effects of sorafenib and/or rapamycin on the growth of subcutaneous xenograft tumors, 50 mg/kg sorafenib tosylate (30% capsitol in water) and 5 mg/kg rapamycin (Rapamune, Wyeth Pharmaceuticals Co.) were orally administered via gavage (200 μl) for 50 days as previously described (18-20). Treatment started on day 7 after transplantation. Tumor growth was monitored every 8 or 14 days.

Proliferation assay: Non-transformed PIL-4 cells, CD133+/CD49f– or CD133–/CD49f– control or TICs were infected with a lentiviral vector expressing GFP and shRNA targeting cellular genes (Open Biosystems). As a control, scrambled shRNA was used. Cell proliferation rate was assessed by incorporation of ^{3}H-uridine in DNA of infected cells (1×10^{3}) seeded in 96-well microplates in complete Williams E culture medium. The cells showed more than 90% transduction rate after 48 hr. Efficiency of knockdown was assessed by qPCR for target genes. *In vivo* assay, BrdU (100mg/kg body weight; Sigma-Aldrich) was injected (i.p.) into mice six hours before mice were sacrificed to assess its incorporation into DNA by immunostaining (21).

***In vitro* invasion assay:** To test invasion activity, a Biocoat Matrigel Invasion Chamber (BD Biosciences Labware) was used as previously described (22). The lower chambers were filled with DMEM/F12, supplemented with 5% calf serum. PIL-4 cells were placed into the upper component of the chamber. After incubation for 22 h at 37 °C, filters were removed, fixed with methanol, and stained with toluidine blue to assess invasion activity. Each assay was set up in triplicate, and all data were analyzed statistically by the *t*-test.

Serial transplantation assay to test cancer-initiating property: To further validate the notion that NANOG^{high}/CD133+/CD49f+ are TICs, these cells and NANOG^{low}/CD133–/CD49f+ control cells were serially transplanted into NOG mice. The two cell populations were first infected with a lentiviral vector expressing GFP to allow for *in vivo* imaging, and were then subcutaneously transplanted with Matrigel into the mice. Tumor incidence and growth were monitored by whole animal GFP imaging. Gross observation and digital photographs of the excised whole liver determined presence, size, and number of liver tumors, when the mice were sacrificed at day 56. NANOG^{high}/CD133+/CD49f+ and NANOG^{low}/CD133–/CD49f+ control cells were isolated from liver tumors and re-transplanted into a new group of recipient mice, and this procedure was repeated once more.

GFP and luciferase imaging analysis: Tumor progression was monitored by whole-body GFP imaging, utilizing the bioluminescence imaging system (IVIS system, Xenogen) every 14 days as previously described (Ref?). Images were captured directly on a microcomputer or continuously through video output on a high resolution VCR (Xenogen). Imaging at lower magnification that visualizes the entire animal was carried out in a light box illuminated by blue light fiber optics (Xenogen, Inc.), and images were recorded by the thermoelectrically cooled color CCD camera. Tumor volume (mm^3) was calculated by the three dimensional animal imaging system at USC Molecular Imaging Center. In the case that a subcutaneous tumor was obvious, tumor volume was measured on the image by caliper and calculated according to the formula $V=0.5\times a^2\times b$, where a is the smallest superficial diameter and b is the largest superficial diameter (23).

The latency period for tumor formation and the tumor size computed from captured 3-D images were compared between animals transplanted with gene manipulated and mock transduced TICs. Groups transplanted with control cells, which were transduced with the above vectors were also included. At the terminal point, animals were sacrificed, and tumors were collected and measured for the actual volume and weight.

Tumor collection and analysis: At 88 days, animals were sacrificed and tumors were collected and measured for the actual volume and weight. Tumor tissues were divided and snap-frozen for mRNA and protein analysis, fixed with 3% paraformaldehyde followed by sucrose treatment for immunostaining to detect GFP and target oncogene products, and fixed with neutrally buffered 10% formalin for H&E staining and histological evaluation.

***In vivo* BrdU staining:** The proliferation rate of the tumor cells was assessed by DNA synthesis rates, as determined by incorporation of bromodeoxyuridine (BrdU) *in vivo*. BrdU (100mg/kg body weight; Sigma-Aldrich) was injected (i.p.) into mice six hours before mice were sacrificed to assess its incorporation into DNA by immunostaining (21).

Histology and immunohistochemistry: Mouse livers from different genetic and treatment groups were fixed in neutrally buffered 4% paraformaldehyde at 4°C and processed for paraffin embedding. Five μm sections were stained with hematoxylin and eosin (H&E). The H&E-stained slides were blindly examined for histology by a board-certified pathologist. TUNEL staining was performed using the in situ cell death detection kit (Roche). Immunohistochemistry staining of cryosections or paraffin sections was performed using antibodies against Nanog (Rabbit #3580, Cell Signalling), p-Smad2/3 (Goat polyclonal antibody, #11769 Santa Cruz), Yap1 (Rabbit #4912, Cell Signalling), Yap1 (Goat polyclonal antibody, #SC17141, Santa Cruz), TLR4 (Mouse monoclonal antibody, SC293072, Santa Cruz), TLR4 (HTA125, eBioscience), IMP3 (IGF2BP3) (Rabbit polyclonal antibody, ab82044, Abcam), based on the standard protocol with mounting media including DAPI for nuclei counterstaining (Vector Laboratories) according to the manufacturer's recommendations. The staining was subjected to morphometric analysis. To determine specificity of immunofluorescent staining, serial sections were similarly processed except primary antibodies were omitted in controls. Fluorescence images were captured on a Zeiss confocal microscope LSM510, using sequential acquisition to give separate image files. The degree of staining was categorized by the extent and intensity of the staining. Image analysis of nuclear translocation was performed using Metamorph or ImageJ v3.91 software (http://rsb.info.nih.gov/ij). Ten high power fields were selected for analysis of each stain. To avoid being biased by the YAP1 and IGF2BP3 staining, each field was selected by viewing nuclear (DAPI) staining only to identify near-confluent cells and thereby maximize the cell numbers included in the analysis. The sections were then evaluated and photographed under a fluorescence microscope and expression of YAP1 and IGF2BP3 were correlated. Quantitative fluorescence data were exported from ImageJ generated histograms into Microsoft Excel software for further analysis and presentation.

Immunohistochemical evaluation: Two independent observers screened all sections for semiquantitative evaluation of NANOG and IGF2BP3/YAP1 immunostaining. The immunoreactive score was determined by the sum of extension and intensity as reported previously (24). Briefly, the intensity of staining was scored on a scale of 0 to 3, in which 0 = negative staining, 1 = weakly positive staining, 2 = moderately positive staining, and 3 = strongly positive staining. The extent of positivity ("extent of distribution" of positive cells) was estimated on a scale of 0 to 4, in which 0 = negative, 1 = positive staining in 0.01-1.0% of cells, 2 = positive staining in 1.01-2.0%; 3 = positive staining in 2.01-3.0%; and 4 = positive staining in more than 3.0%. The results were evaluated as immunoreactivity score, where the immunoreactivity score = [percentage of positive cells (score 0-4)] × [(staining intensity (score 0 to 3)] (24). The combined immunoreactivity score (percentage × intensity) ≥2 was considered as positive staining. Two investigators separately and independently evaluated the immunohistochemical staining without knowledge of the clinical data. Significant differences in interpretation were resolved in conference. In cases without significant discordance, scores of two observers were averaged.

Reverse transcription-PCR (RT-PCR): Livers or cells were lysed with TRI reagent (Molecular Research Center). To demonstrate the specific detection of NANOGP8, the specificity was established by qRT-PCR primers, which recognize the 3'UTR region of NANOG but not

NANOGP8 (6). Relative quantitative PCR was performed on a 7500 Fast Real-Time PCR System (Applied Biosystems) using SYBR Green PCR mix (Applied Biosystems). Cycle conditions were as follows: 1 cycle at 50°C for 2 minutes, followed by 1 cycle at 95°C for 10 minutes, followed by 40 cycles at 95°C for 15 seconds and 60°C for 1 minute. Specificity of PCR products was tested by dissociation curves. Threshold cycles of primer probes were normalized to *Gapdh*. Relative values of transcripts were calculated using the equation, $2^{-\Delta}Ct$, where ΔCt is equal to the difference in threshold cycles for target and reference.
The following primer pairs were used as previously described (25-30).

Gene	Primer
Human *Albumin*	F : 5'-CATGCCAAATTAGTGCAGGA-3' R : 5'-GCTGGGGTTGTCATCTTTGT-3'(25)
Human *Cytokeratin 19* (*Ck19*)	F : 5'-TGCTGGATGAGCTGACTCTG-3' R : 5-AATCCACCTCCACACTGACC-3'(31)
Human *Cd133* (*Prom1*)	F : 5'-TCATCGCTGTGGTCGTCATTG-3' R : 5'-GTCCGCTGGTGTAGTGTTGTAG-3'(32)
Human *Nanog*	F : 5'-TGAACCTCAGCTACAAACAG-3' R : 5'-TGGTGGTAGGAAGAGTAAAG-3'(30)
Human *Oct4*	F : : 5'-AGCGAACCAGTATCGAGAAC-3' R : 5'-TTACAGAACCACACTCGGAC-3'(30)
Human *Sox2*	F : 5'-AGCTACAGCATGATGCAGGGA-3' R : 5'-GGTCATGGAGTTGTACTGCA-3'(26, 30)
Human *Epcam*	F : 5'-CGCAGCTCAGGAAGAATGTG-3' R : 5'-TGAAGTACACTGGCATTGACG-3'(28)
Human *Afp*	F : 5'-GCAAAGCTGAAAATGCAGTTGA-3' R : 5'-GGAAAGTTCGGGTCCCAAAA-3'(27)
Human *Igf2bp3*	F : 5′-AGTTGTTGTCCCTCGTGACC-3′ R : 5′-GTCCACTTTGCAGAGCCTTC-3′ (33)
Human *Yap1*	F : 5'-CCTTCTTCAAGCCGCCGGAG-3' R : 5'-CAGTGTCCCAGGAGAAACAGC-3'(34)
Human *Gapdh*	F : 5'- ACCACAGTCCATGCCATCAC-3' R : 5'- TCCACCACCCTGTTGCTGTA-3'(25)
Mouse *Alb*	F : *5'*-CATGACACCATGCCTGCTGAT-3' R: 5'-GCCTTTCCACCAGGGATCCAC-3'(35)
Mouse *Ck19*	F : *5'*-GTCCTACAGATTGACAATG-3' R: 5'-CACGCTCTGGATCTGTGACAG-3'(35)
Mouse *Cd133*	F : 5'-CTGGGAGGCAGAATAAAGGA-3' R: 5'-GGTTGGTATTGAGCTGGGTG-3'(29)
Mouse *Nanog*	F : 5'-AGGGTCTGCTACTGAGATGCTCTG-3' R : 5'-CAACCACTGGTTTTTCTGCCACCG-3'(26)
Mouse *Oct4*	F : 5'-CTGTAGGGAGGGCTTCGGGCACTT-3' R: 5'-CTGAGGGCCAGGCAGGAGCACGAG-3'(26)
Mouse *Sox2*	F : 5'-GGCAGCTACAGCATGATGCAGGAGC-3' R: 5'-CTGGTCATGGAGTTGTACTGCAGG-3' (26)
Mouse *Epcam*	F : *5'*-CGGCTCAGAGAGACTGTGTC-3' R: 5'-GATCCAGTAGGTCCTCACGC-3'(35)
Mouse *Afp*	F : 5'-CTGGAGTGTCTGCAGGATGG-3' R: 5'-CCACAGCCGGACCATTTCTC-3'(35)
Mouse *Tlr4*	F : 5'-GGC AAC TTG GAC CTG AGG AG-3' R: 5'-CAT GGG CTC TCG GTC CAT AG-3'(36)
Mouse *Igf2bp3*	F : 3'-CCTTTGCTGCTGGCAGAGTT-3' R : 5'-AACAAAGGGAAGTGCAGAGC-3' (37)
Mouse *Yap1*	F : 5′-CAGGAATTATTTCGGCAGGA-3' R : , 5′-CATCCTGCTCCAGTGTAGGC-3′ (38)

Mouse *Gapdh*	F : 5'-GCACAGTCAAGGCCGAGAAT-3' R : 5'-GCCTTCTCCATGGTGGTGAA-3'(26)

Supplementary References

1. Majumder, M., Steele, R., Ghosh, A.K., Zhou, X.Y., Thornburg, L., Ray, R., Phillips, N.J., and Ray, R.B. 2003. Expression of hepatitis C virus non-structural 5A protein in the liver of transgenic mice. *FEBS Lett* 555:528-532.
2. Tang, Y., Katuri, V., Dillner, A., Mishra, B., Deng, C.X., and Mishra, L. 2003. Disruption of transforming growth factor-beta signaling in ELF beta-spectrin-deficient mice. *Science* 299:574-577.
3. Jellicoe, M.M., Nichols, S.J., Callus, B.A., Baker, M.V., Barnard, P.J., Berners-Price, S.J., Whelan, J., Yeoh, G.C., and Filipovska, A. 2008. Bioenergetic differences selectively sensitize tumorigenic liver progenitor cells to a new gold(I) compound. *Carcinogenesis* 29:1124-1133.
4. Libbrecht, L., Desmet, V., Van Damme, B., and Roskams, T. 2000. The immunohistochemical phenotype of dysplastic foci in human liver: correlation with putative progenitor cells. *J Hepatol* 33:76-84.
5. Libbrecht, L., De Vos, R., Cassiman, D., Desmet, V., Aerts, R., and Roskams, T. 2001. Hepatic progenitor cells in hepatocellular adenomas. *Am J Surg Pathol* 25:1388-1396.
6. Jeter, C.R., Badeaux, M., Choy, G., Chandra, D., Patrawala, L., Liu, C., Calhoun-Davis, T., Zaehres, H., Daley, G.Q., and Tang, D.G. 2009. Functional evidence that the self-renewal gene NANOG regulates human tumor development. *Stem Cells* 27:993-1005.
7. Saitoh, S., Akashi, S., Yamada, T., Tanimura, N., Kobayashi, M., Konno, K., Matsumoto, F., Fukase, K., Kusumoto, S., Nagai, Y., et al. 2004. Lipid A antagonist, lipid IVa, is distinct from lipid A in interaction with Toll-like receptor 4 (TLR4)-MD-2 and ligand-induced TLR4 oligomerization. *Int Immunol* 16:961-969.
8. Kotani, K., Ogawa, W., Hino, Y., Kitamura, T., Ueno, H., Sano, W., Sutherland, C., Granner, D.K., and Kasuga, M. 1999. Dominant negative forms of Akt (protein kinase B) and atypical protein kinase Clambda do not prevent insulin inhibition of phosphoenolpyruvate carboxykinase gene transcription. *J Biol Chem* 274:21305-21312.
9. Chambers, I., and Tomlinson, S.R. 2009. The transcriptional foundation of pluripotency. *Development* 136:2311-2322.
10. Loh, Y.H., Wu, Q., Chew, J.L., Vega, V.B., Zhang, W., Chen, X., Bourque, G., George, J., Leong, B., Liu, J., et al. 2006. The Oct4 and Nanog transcription network regulates pluripotency in mouse embryonic stem cells. *Nat Genet* 38:431-440.
11. Chen, X., Xu, H., Yuan, P., Fang, F., Huss, M., Vega, V.B., Wong, E., Orlov, Y.L., Zhang, W., Jiang, J., et al. 2008. Integration of external signaling pathways with the core transcriptional network in embryonic stem cells. *Cell* 133:1106-1117.
12. Mitsui, K., Tokuzawa, Y., Itoh, H., Segawa, K., Murakami, M., Takahashi, K., Maruyama, M., Maeda, M., and Yamanaka, S. 2003. The homeoprotein Nanog is required for maintenance of pluripotency in mouse epiblast and ES cells. *Cell* 113:631-642.
13. Kim, M.K., Shin, J.M., Eun, H.C., and Chung, J.H. 2009. The role of p300 histone acetyltransferase in UV-induced histone modifications and MMP-1 gene transcription. *PLoS One* 4:e4864.
14. Kopp, J., Preis, E., Said, H., Hafemann, B., Wickert, L., Gressner, A.M., Pallua, N., and Dooley, S. 2005. Abrogation of transforming growth factor-beta signaling by SMAD7 inhibits collagen gel contraction of human dermal fibroblasts. *J Biol Chem* 280:21570-21576.
15. Dooley, S., Delvoux, B., Streckert, M., Bonzel, L., Stopa, M., ten Dijke, P., and Gressner,

A.M. 2001. Transforming growth factor beta signal transduction in hepatic stellate cells via Smad2/3 phosphorylation, a pathway that is abrogated during in vitro progression to myofibroblasts. TGFbeta signal transduction during transdifferentiation of hepatic stellate cells. *FEBS Lett* 502:4-10.

16. Yang, Z.F., Ho, D.W., Ng, M.N., Lau, C.K., Yu, W.C., Ngai, P., Chu, P.W., Lam, C.T., Poon, R.T., and Fan, S.T. 2008. Significance of CD90+ cancer stem cells in human liver cancer. *Cancer Cell* 13:153-166.
17. Yang, Z.F., Poon, R.T., Luo, Y., Cheung, C.K., Ho, D.W., Lo, C.M., and Fan, S.T. 2004. Up-regulation of vascular endothelial growth factor (VEGF) in small-for-size liver grafts enhances macrophage activities through VEGF receptor 2-dependent pathway. *J Immunol* 173:2507-2515.
18. Huynh, H., Ngo, V.C., Koong, H.N., Poon, D., Choo, S.P., Thng, C.H., Chow, P., Ong, H.S., Chung, A., and Soo, K.C. 2009. Sorafenib and rapamycin induce growth suppression in mouse models of hepatocellular carcinoma. *J Cell Mol Med* 13:2673-2683.
19. Wang, Z., Zhou, J., Fan, J., Qiu, S.J., Yu, Y., Huang, X.W., and Tang, Z.Y. 2008. Effect of rapamycin alone and in combination with sorafenib in an orthotopic model of human hepatocellular carcinoma. *Clin Cancer Res* 14:5124-5130.
20. Newell, P., Toffanin, S., Villanueva, A., Chiang, D.Y., Minguez, B., Cabellos, L., Savic, R., Hoshida, Y., Lim, K.H., Melgar-Lesmes, P., et al. 2009. Ras pathway activation in hepatocellular carcinoma and anti-tumoral effect of combined sorafenib and rapamycin in vivo. *J Hepatol* 51:725-733.
21. Zheng, Y., Chen, W.L., Louie, S.G., Yen, T.S., and Ou, J.H. 2007. Hepatitis B virus promotes hepatocarcinogenesis in transgenic mice. *Hepatology* 45:16-21.
22. Albini, A., Iwamoto, Y., Kleinman, H.K., Martin, G.R., Aaronson, S.A., Kozlowski, J.M., and McEwan, R.N. 1987. A rapid in vitro assay for quantitating the invasive potential of tumor cells. *Cancer Res* 47:3239-3245.
23. Machida, K., Tsukamoto, H., Mkrtchyan, H., Duan, L., Dynnyk, A., Liu, H.M., Asahina, K., Govindarajan, S., Ray, R., Ou, J.H., et al. 2009. Toll-like receptor 4 mediates synergism between alcohol and HCV in hepatic oncogenesis involving stem cell marker Nanog. *Proc Natl Acad Sci U S A* 106:1548-1553.
24. Koomagi, R., and Volm, M. 1999. Expression of Fas (CD95/APO-1) and Fas ligand in lung cancer, its prognostic and predictive relevance. *Int J Cancer* 84:239-243.
25. Tanimizu, N., Saito, H., Mostov, K., and Miyajima, A. 2004. Long-term culture of hepatic progenitors derived from mouse Dlk+ hepatoblasts. *J Cell Sci* 117:6425-6434.
26. Chen, S., Do, J.T., Zhang, Q., Yao, S., Yan, F., Peters, E.C., Scholer, H.R., Schultz, P.G., and Ding, S. 2006. Self-renewal of embryonic stem cells by a small molecule. *Proc Natl Acad Sci U S A* 103:17266-17271.
27. Rao, M.S., Khan, A.A., Parveen, N., Habeeb, M.A., Habibullah, C.M., and Pande, G. 2008. Characterization of hepatic progenitors from human fetal liver during second trimester. *World J Gastroenterol* 14:5730-5737.
28. Kimura, H., Kato, H., Faried, A., Sohda, M., Nakajima, M., Fukai, Y., Miyazaki, T., Masuda, N., Fukuchi, M., and Kuwano, H. 2007. Prognostic significance of EpCAM expression in human esophageal cancer. *Int J Oncol* 30:171-179.
29. Wu, A., Oh, S., Wiesner, S.M., Ericson, K., Chen, L., Hall, W.A., Champoux, P.E., Low, W.C., and Ohlfest, J.R. 2008. Persistence of CD133+ cells in human and mouse glioma cell lines: detailed characterization of GL261 glioma cells with cancer stem cell-like properties. *Stem Cells Dev* 17:173-184.
30. Park, I.H., Zhao, R., West, J.A., Yabuuchi, A., Huo, H., Ince, T.A., Lerou, P.H., Lensch, M.W., and Daley, G.Q. 2008. Reprogramming of human somatic cells to pluripotency with defined factors. *Nature* 451:141-146.

31. Rountree, C.B., Senadheera, S., Mato, J.M., Crooks, G.M., and Lu, S.C. 2008. Expansion of liver cancer stem cells during aging in methionine adenosyltransferase 1A-deficient mice. *Hepatology* 47:1288-1297.
32. Snippert, H.J., van Es, J.H., van den Born, M., Begthel, H., Stange, D.E., Barker, N., and Clevers, H. 2009. Prominin-1/CD133 marks stem cells and early progenitors in mouse small intestine. *Gastroenterology* 136:2187-2194 e2181.
33. Liao, B., Hu, Y., Herrick, D.J., and Brewer, G. 2005. The RNA-binding protein IMP-3 is a translational activator of insulin-like growth factor II leader-3 mRNA during proliferation of human K562 leukemia cells. *J Biol Chem* 280:18517-18524.
34. Zhang, J., Ji, J.Y., Yu, M., Overholtzer, M., Smolen, G.A., Wang, R., Brugge, J.S., Dyson, N.J., and Haber, D.A. 2009. YAP-dependent induction of amphiregulin identifies a non-cell-autonomous component of the Hippo pathway. *Nat Cell Biol* 11:1444-1450.
35. Okabe, M., Tsukahara, Y., Tanaka, M., Suzuki, K., Saito, S., Kamiya, Y., Tsujimura, T., Nakamura, K., and Miyajima, A. 2009. Potential hepatic stem cells reside in EpCAM+ cells of normal and injured mouse liver. *Development* 136:1951-1960.
36. Nhu, Q.M., Cuesta, N., and Vogel, S.N. 2006. Transcriptional regulation of lipopolysaccharide (LPS)-induced Toll-like receptor (TLR) expression in murine macrophages: role of interferon regulatory factors 1 (IRF-1) and 2 (IRF-2). *J Endotoxin Res* 12:285-295.
37. Monk, D., Bentley, L., Beechey, C., Hitchins, M., Peters, J., Preece, M.A., Stanier, P., and Moore, G.E. 2002. Characterisation of the growth regulating gene IMP3, a candidate for Silver-Russell syndrome. *J Med Genet* 39:575-581.
38. Fernandez, L.A., Northcott, P.A., Dalton, J., Fraga, C., Ellison, D., Angers, S., Taylor, M.D., and Kenney, A.M. 2009. YAP1 is amplified and up-regulated in hedgehog-associated medulloblastomas and mediates Sonic hedgehog-driven neural precursor proliferation. *Genes Dev* 23:2729-2741.